Computed Euler Flowfield for a Transonic Aircraft with Stores

J. H. Fox,* T. L. Donegan,† J. L. Jacocks,‡ and R. H. Nichols†
Arnold Engineering Development Center, Arnold Air Force Base, Tennessee 37389

A series of computations solving the Euler equations that model the flowfield produced by the F-15E aircraft flying at a Mach number of 0.98 has been completed. Three configurations were simulated. The most complex configuration consisted of a wing-body combination with an ingesting inlet, pylon system, a targeting pod with pylon, and a finned store in carriage position. This required 29 grids and subgrids with a total of 1.2×10^6 mesh points. Results generally compared favorably with wind-tunnel measurements of surface pressure and with a cone-probe survey of the pressure field proximate to the store carriage position. The trajectory of the finned store was well predicted.

Introduction

THE F-15E is the long-range, dual-role version of the F-15 air-superiority aircraft. Large conformal fuel tanks (CFTs) attached at the wing/inlet juncture (Fig. 1) provide the increased range. Hardened locations on the CFTs provide attachment points for the pylon/store system. Stores released from the pylons must fall cleanly and leave the near field of the craft in an attitude that allows a proper trajectory.

Currently, the wind-tunnel/flight test program intended to ensure that a store will release properly is lengthy and costly. It may involve 20 flight tests, one or two wind-tunnel entries, and extend over a period of two years. In the event of an improper trajectory, pylon and/or attachment point modifications may have to be made resulting in more flight and wind-tunnel testing. The purpose of the present undertaking was to determine whether computational fluid dynamics had matured sufficiently to provide a viable supplement to the wind tunnel. In particular, this effort was developed to determine if computed flowfield data would be of sufficient quality to serve to reduce the test matrix and supplement the measured data such that additional testing could be reduced or eliminated. Further, it was anticipated that computed flowfields could serve as a diagnostic aid in deciding among possible solutions to design problems. Therefore, a complex configuration was chosen: the F-15E with a nearly complete pylon system, an attached targeting pod, a wing, an inlet with correct mass flow-rate ingestion, and one guided store with forward-mounted canards and rear-mounted fin gloves (the fins to be extended after release). This configuration was chosen because it had a considerable amount of measured data available, its geometry was available, and there was an ongoing testing program in place that would allow further opportunities for demonstration.

Configurations

The numbers of components listed are half of the complement present on the actual aircraft because of the assumption of symmetry.

Configuration 1. The first configuration consists of the basic model with attached CFT, inlet with scaled mass flow rate, and wing.

Configuration 2. The second configuration is the same as configuration 1, except that three stub pylons are attached outboard and one long pylon attached inboard on the CFT, a pylon is attached to the wing, and a pylon is located on the centerline of the fuselage. A model of the targeting pod is attached to its own pylon, as in Fig. 1. (Because of the symmetry assumption, the shape of the targeting pod will necessarily be the shape of the navigation pod, which is the corresponding component across the aircraft centerline.)

Configuration 3. The third configuration is the same as configuration 2 with the addition of the guided store attached to the forward-most outboard stub pylon shown in Fig. 1. Store canards were fixed and not free to weathercock in either the wind-tunnel tests or the computations.

Approach to Numerical Solution

General

Grid generation looms as the most daunting obstacle when considering computing the flowfield about complex geometries having disparate components with different topologies. There is little choice but to use a domain decomposition methodology that allows the development of the various grids as independently from other grids as possible, so that the grid generation effort may be done in parallel by various workers.

This requirement effectively eliminates techniques that require common boundaries between grids. The embedding method of Benek et al.[1] has proved to be the most practical for team use in external flow studies at the Arnold Engineering Development Center (AEDC), particularly since it is well

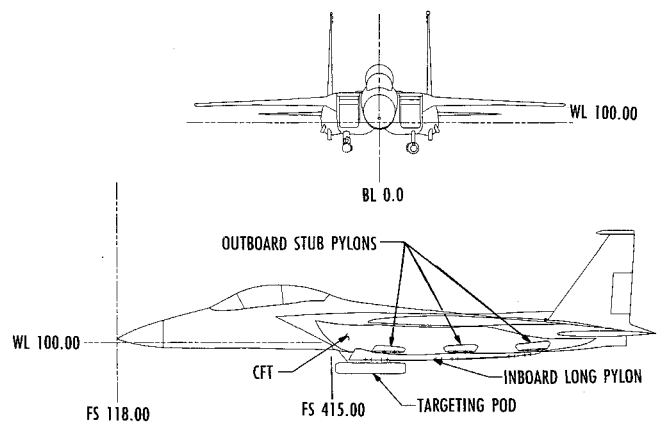

Fig. 1 Configuration 2, not shown are wing and centerline pylons.

Presented as Paper 89-2219 at the AIAA 27th Applied Aerodynamics Conference, Seattle, WA, July 31–Aug. 2, 1989; received April 2, 1990; revision received June 18, 1990; accepted for publication June 18, 1990.

*Principal Research Engineer A, Calspan Corporation, Arnold Engineering Development Center Operations, Aerospace Systems Facility. Associate Fellow AIAA.

†Senior Research Engineer, Calspan Corporation, Arnold Engineering Development Center Operations, Aerospace Systems Facility. Member AIAA.

‡Executive Engineer, Calspan Corporation, Arnold Engineering Development Center Operations, Aerospace Systems Facility. Senior Member AIAA.

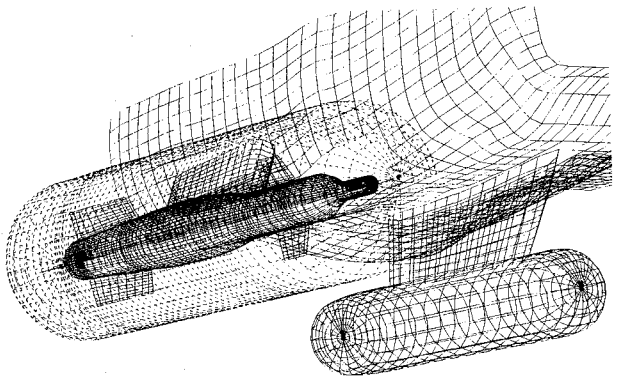

Fig. 2 Configuration 3 showing store grid.

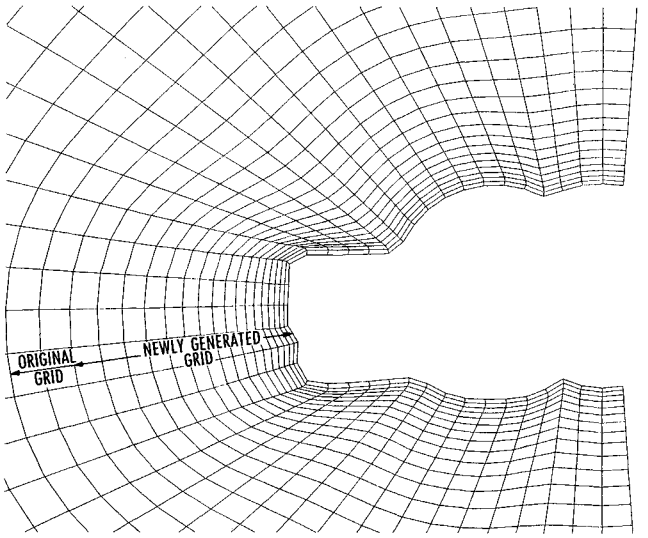

Fig. 3 Typical cut of fuselage grid.

documented and a continuing effort is in place to upgrade the technology. The most recent work in this regard is Dietz et al.[2]

Numerical Algorithm

The implicit, approximate factorization scheme of Beam and Warming[3] was used to solve the time-dependent Euler equations in a curvilinear coordinate system that is boundary conforming. The coded form of the scheme is coupled to Benek's domain decomposition technique. Benek based his solver on the work of Pulliam and Steger.[4]

Overview of Grid Development

Model fidelity was sacrificed to simplify grid generation when the effects were judged to be minor. The aft portion of the aircraft was straightened and the tail surfaces eliminated. Also, the boundary-layer diverter between the fuselage and inlet and the aft outboard pylon were both omitted from the computational configurations. A minor change to the finned store was that the seeker, a conically shaped device attached to the nose of the store, was faired over.

Grid development followed a simple pattern. Separate coarse grids were generated about the fuselage and the wing. Refined subgrids were then generated for the fuselage and the wing to provide transition from the much finer grids of the pylons. Grid generation for the wing, stores, and pylons occurred independently, but in parallel, with the fuselage grid generation effort. (Depicted in Fig. 2 is the outline of the grid encompassing the store in configuration 3. For clarity, some of the grids shown are coarser than actually used in the computations.) Once the store and pylon grids and the fuselage subgrids were constructed, they were assembled and the interpolation coefficients computed and stored using the assembly routine of Ref. 2. The stored interpolation coefficients were used to provide boundary conditions for the interacting grids, and the flow tangency condition was used on solid surfaces.

For reference in the following discussion, the Cartesian coordinates are x, axially, increasing aft; y, parallel to the planform of the wing and positive to the pilot's right; and z, normal to the x-y plane, parallel to the symmetry plane, and positive upward. Flowfield variables are the following: density ρ; the three Cartesian velocity components u, v, and w, which are aligned respectively with the x, y, and z coordinates; and total energy e. All dimensions shown are in full-scale inches.

Grid Embedding

The grid embedding method of domain decomposition[1] was developed to simplify the development of grids about configurations containing disparate geometries. The method subdivides the physical domain into regions that contain locally optimized grids. A complex configuration such as the F-15E requires grids of both spherical and cylindrical topologies. Since each grid is optimized to a particular geometrical element, each grid may have parts of itself contained within neighboring grids. Thus, domain decomposition techniques must introduce boundaries into the computational domain. These new boundaries define the subdomains in regions interior to the undivided domain. Boundary data are supplied to these boundaries by trilinear interpolations within other interacting meshes. In the embedding scheme of Ref. 1, two types of boundaries are allowed: outer boundaries and hole boundaries. Holes are introduced to eliminate grid points that are contained within solid bodies and, hence, lie outside the computational domain. Since these boundaries are not at the extrema of the indices, they are imposed by blanking out the appropriate equations within the solution matrix and directly substituting the boundary condition. This procedure effectively partitions the matrix. Mesh points within a hole are similarly blanked.

Communication among the grids is of such complexity that a separate preprocessor accomplishes this task. A discussion of the methodologies used to tag hole boundary points and

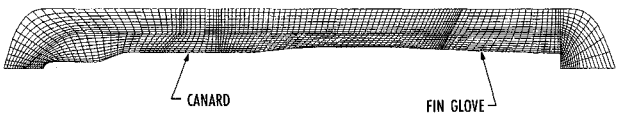

Fig. 4 Meridian plane of store grid through forward canard and rear fin glove.

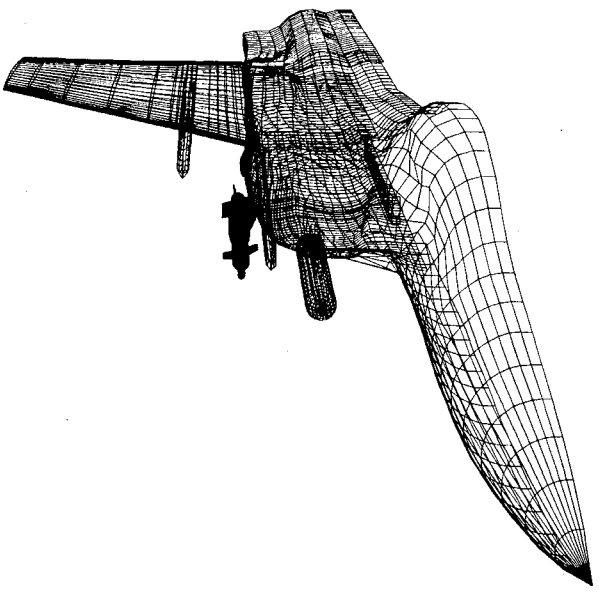

Fig. 5 Complete ensemble of surface grids.

outer boundary points and to provide the interpolation coefficients is contained in Ref. 2. The primary limitation placed on the separate grid generation processes was storage. This limited each grid to a maximum of about 80,000 points, which generally translated into 61 points in the principal flow direction x, 41 points azimuthally, and 31 points outward in the direction generally normal to the surface of the geometrical element being considered.

Grid Generation

Four grid generation techniques were employed for the building of grids: elliptic generation,[5] algebraic generation, manual specification and insertion, and a method that combined the three with an enforcement of body-normal conditions on solid surfaces. This combination method is referred to as the displaced-surface/spline-fit method and warrants a brief description.

An initial grid was generated by using the Poisson solver for only a few iterations or, in many cases, an algebraic grid sufficed. Skewness would still be apparent at the solid surface. Points near the surface were discarded. A second surface was constructed offset from the solid surface; i.e., surface normals were computed on the solid surface, and the surface was displaced along the normals at all points a certain distance. Using a point from the original surface, the corresponding point from the displaced surface, and one to any number of pre-existing points from the same coordinate path of the initial grid, a relaxed spline fit[6] was computed. An interpolation along the fit yielded a new coordinate line. The new coordinate line varied smoothly from the solid surface, maintaining the body-normal condition, out to a point in the initial grid. From this point, the new coordinate line followed the initial grid path to its terminus. Figure 3 depicts a typical cut from the fuselage grid. In this case, an algebraic grid was used for the initial grid.

Inlet

It was necessary to provide a simulation of the inlet flow to model the spillage effect on the nearby store. An inlet mesh was generated that penetrated the aircraft fuselage grid. Mass flow-rate boundary conditions were imposed on the downstream face inside the fuselage. Surfaces of the inlet grid exposed to the flow outside the inlet were provided with boundary conditions by interpolation from the fuselage subgrid. The fuselage surface at the inlet face, in turn, received its boundary conditions from the inlet grid.

Wing, Pylons, and Stores

The wing grid was generated by stacking a series of two-dimensional grids along the span, each of which was generated by a two-dimensional Poisson solver.[5] Storage limitations required that the wing grid be broken into an upper and lower

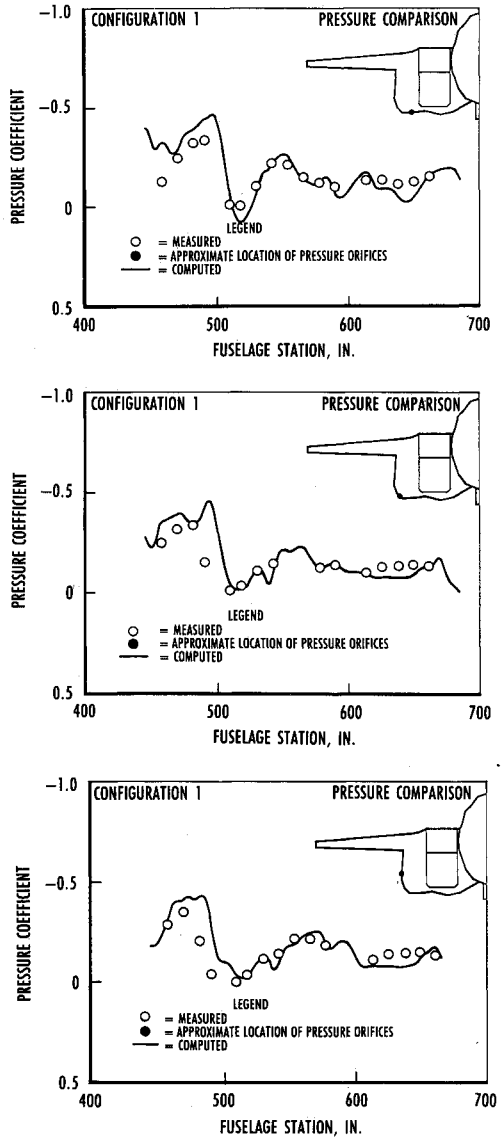

Fig. 6 Surface pressure on CFT, configuration 1.

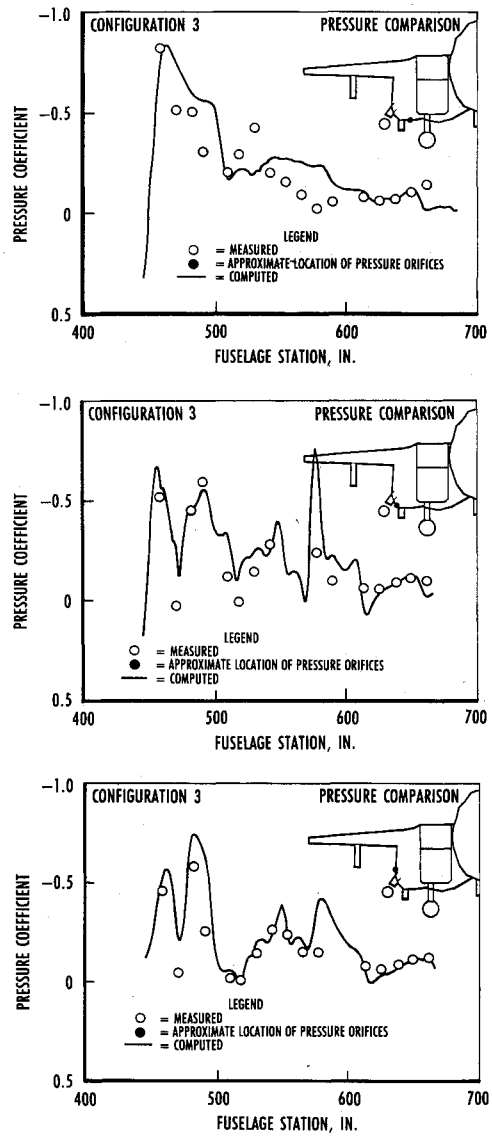

Fig. 7 Surface pressure on CFT, configuration 3.

half that were overlapped by five grid points at both the leading and trailing edges. The stacked set of planes was terminated near the fuselage, and another grid was generated using the displaced-surface/spline-fit method to transition to the fuselage shape.

Computational grids for the pylons were complicated by conflicting resolution requirements: coarseness was required at the root so the fuselage subgrids would not have to be highly refined, but fine mesh spacing was required at the tip to accommodate the mounting of stores. The pylon grids were generated using the expanded-surface/spline-fit method. As with the wing, the juncture was generated separately. Iteration of the juncture grid was usually necessary to assure that the adjoining grids matched well and produced good interpolation coefficients.

The finned store and the targeting pod, being axially symmetric, had their grids generated with a two-dimensional Poisson solver in one meridian plane that was the length of the body. For the targeting pod grid, the two-dimensional plane was simply rotated to generate the full grid. The store, however, was treated somewhat differently to obviate the necessity for generating separate grids for each fin.

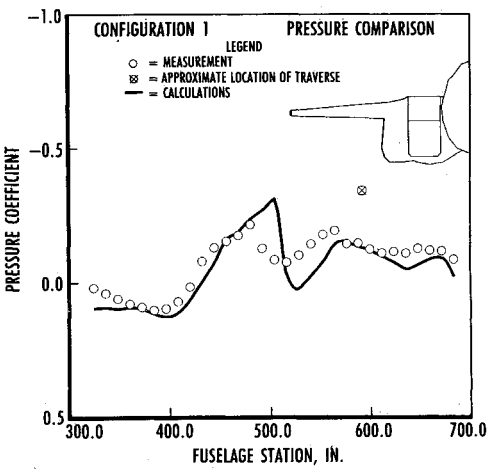

a) Waterline, 54.09; buttline, 96.39

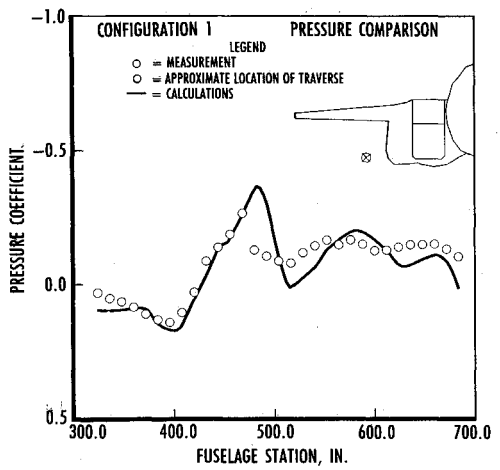

b) Waterline, 90.09; buttline, 96.42

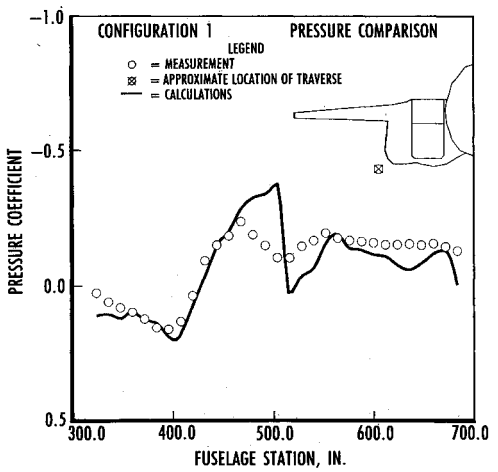

c) Waterline, 78.14; buttline, 84.48

Fig. 8 Pressure at traverse points, configuration 1.

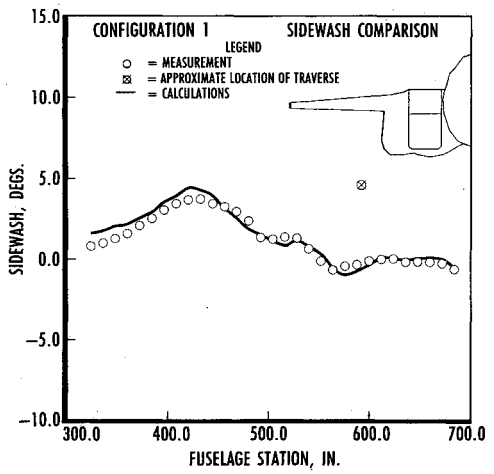

a) Waterline, 54.09; buttline, 96.39

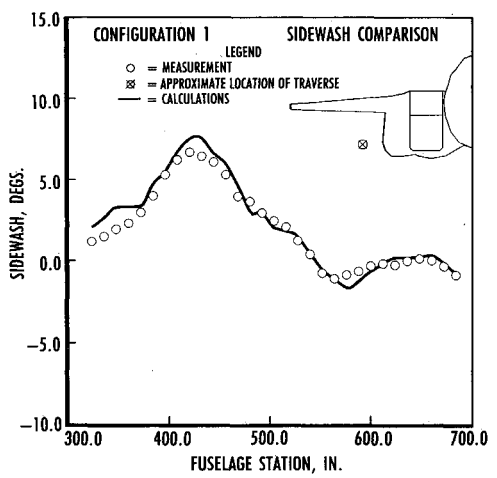

b) Waterline, 90.09; buttline, 96.42

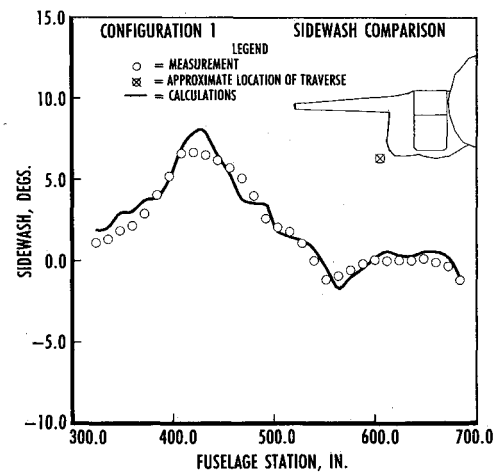

c) Waterline, 78.14; buttline, 84.48

Fig. 9 Sidewash at traverse points, configuration 1.

To preserve the fin planform on the guided store, a two-dimensional grid was created that had grid areas shaped to match the fins and canards, as depicted in Fig. 4. Four circumferentially overlapping grids were constructed to overlap at the fin locations, with zero fin thickness. By aligning field grid areas with the planform of the fins, the correct fin shape was achieved. Tangential flow boundary conditions were imposed directly for each side of the fin, so that each grid contained, say, the left side of one fin and the right side of the next fin. Surface grids for the store, the targeting pod, and their respective pylons are seen in Fig. 2. Storage limitations necessitated further sudivision of the grids into two lengthwise grids for each set of control surfaces (canard forward, fin aft). Figure 5 depicts the ensemble of surface grids for the wing, pylons, and store as attached to the fuselage.

Boundary Conditions and Convergence

The assembly routine of Ref. 2 provided the necessary interpolation coefficients to compute the explicit flow variables on the grid boundaries. At solid surfaces, the flow tangency condition was enforced by setting the normal veloc-

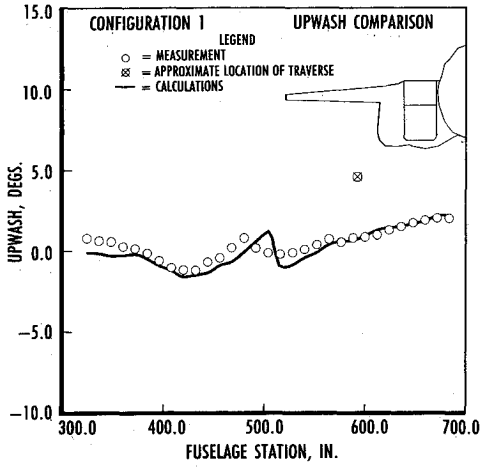

a) Waterline, 54.09; buttline, 96.39

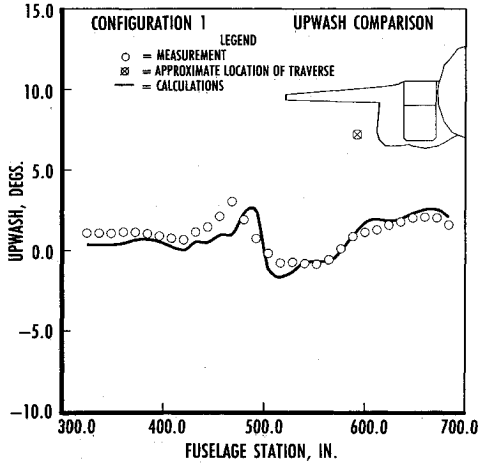

b) Waterline, 90.09; buttline, 96.42

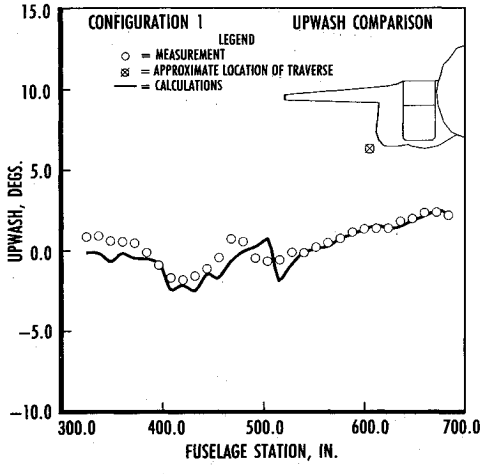

c) Waterline, 78.14; buttline, 84.48

Fig. 10 Upwash at traverse points, configuration 1.

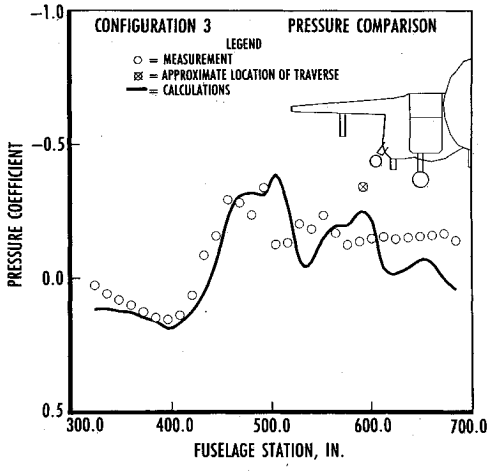

a) Waterline, 54.06; buttline, 96.48

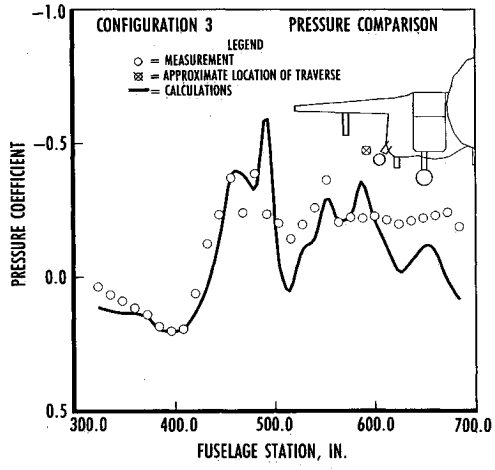

b) Waterline, 90.09; buttline, 96.50

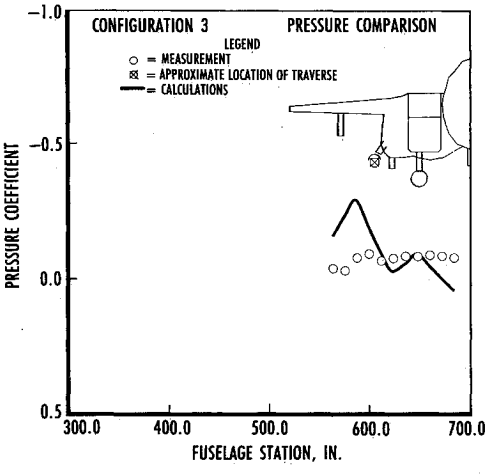

c) Waterline, 78.19; buttline, 84.62

Fig. 11 Pressure at traverse points, configuration 3.

ity component to zero. This was accomplished by first determining the surface-normal component of velocity one grid point away from the solid surface. Next, the normal component was subtracted from the velocity vector at the same point. Finally, a zeroth-order extrapolation was made of the new vector to the surface. Density and pressure were similarly extrapolated to the surface from the first point away, and the total energy was computed at the surface. Nonreflective freestream boundary conditions were used on the outermost boundary of the outermost grid, and lateral symmetry was assumed for the entire configuration. Convergence to steady state was assumed when the l_2 norm of the residuals for each of the grids had decreased three orders of magnitude.

Results and Discussion

Measured data for comparisons were taken from a test run in the 4-ft aerodynamic wind tunnel (4T) at AEDC. A model of the F-15E was tested at a Mach number of 0.98 and an angle of attack of 1.1 deg. The unit Reynolds number was 2×10^6/ft. Static pressure was obtained from three rows of orifices on the side of the CFT, and static pressure, total pressure, and flow angle were measured with a five-hole conical

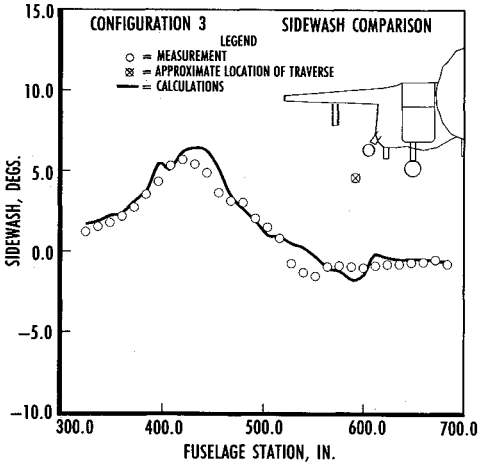

a) Waterline, 54.06; buttline, 96.48

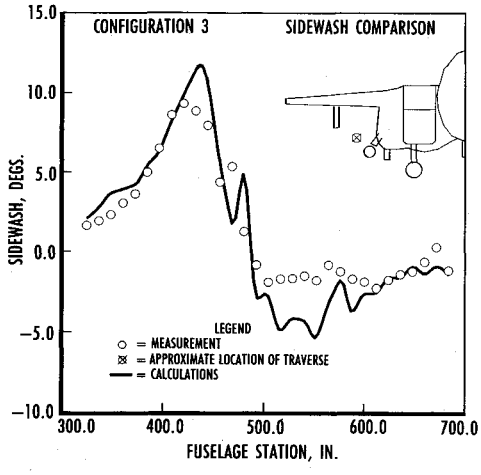

b) Waterline, 90.09; buttline, 96.50

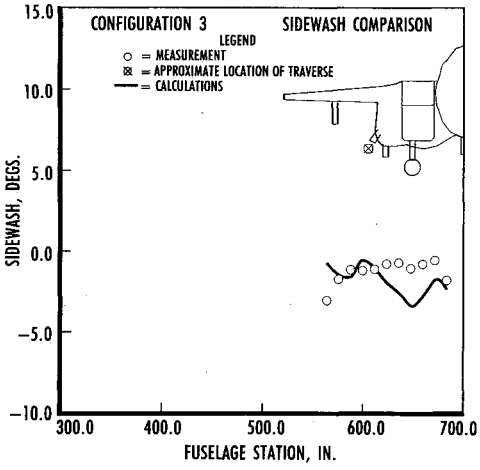

c) Waterline, 78.19; buttline, 84.62

Fig. 12 Sidewash at traverse points, configuration 3.

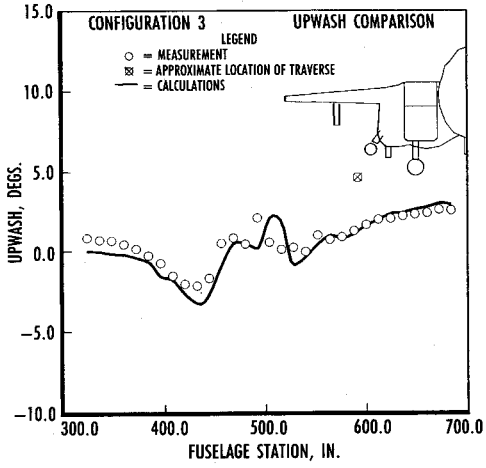

a) Waterline, 54.06; buttline, 96.48

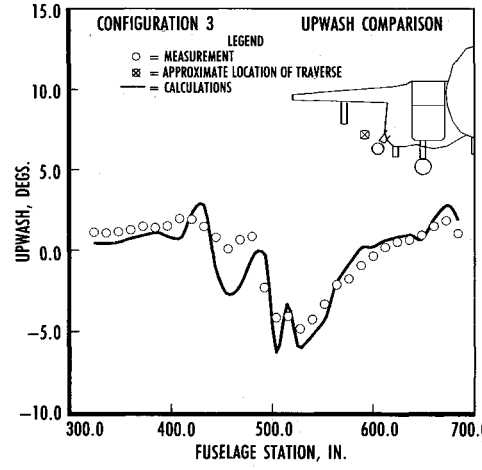

b) Waterline, 90.09; buttline, 96.50

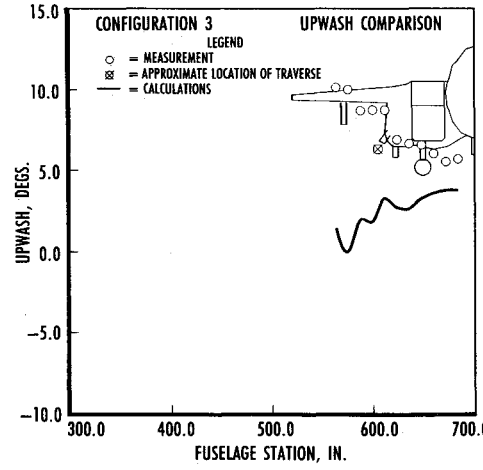

c) Waterline, 78.19; buttline, 84.62

Fig. 13 Upwash at traverse points, configuration 3.

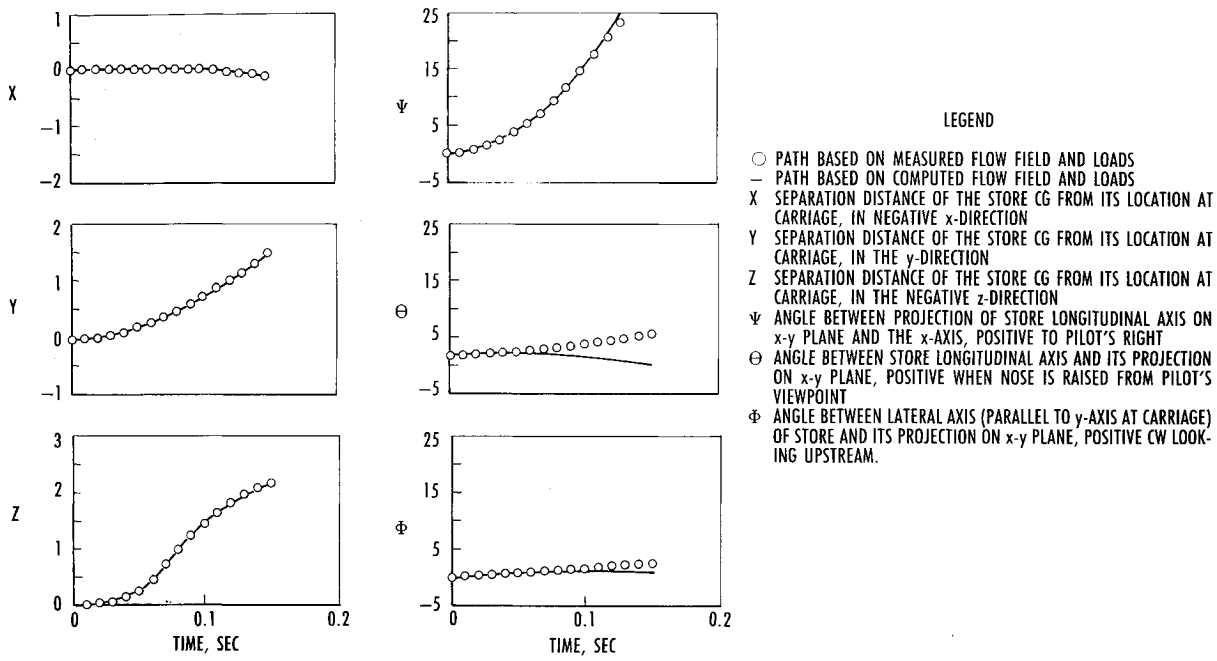

a) Trajectory of store c.g., ft b) Store attitude, deg

Fig. 14 Store trajectory comparison.

probe traversed beneath the fuselage. Flowfields for three configurations were computed; however, only comparisons for configurations 1 and 3 are shown. The comparisons for configuration 2 are similar in character to those of configuration 3.[7] In the computations, the inlet ingestion mass flow rate was taken as 118 lb/s, full scale.

The authors took approximately six months and 2200 man-hours to complete the solutions. Grid development consumed the bulk of that time. With the experience gained and the advent of interactive grid generators,[8] the time for a completely new aircraft has been reduced to about 800 man-hours. A major benefit of the decomposition technique is that stores may be added or removed within a few hours. The Euler solution for configuration 3 required approximately 23 CPU hours on a Cray XMP-12.

Spline fits of the solutions for the two configurations were used to produce the solid curves of surface pressure plotted with the CFT pressure orifice data, Figs. 6 and 7. The curves depicting the computed results in Figs. 8–13 were produced by using a trilinear interpolation of the solution to obtain values at the same locations as the cone-probe traverses.

Agreement between the computed pressure coefficients on the CFT and the measured values are quite good for the clean aircraft, as shown in Fig. 6. The downstream shift of shock waves when compared with 4T data is typical of Euler solutions. However, as indicated in Fig. 7, the addition of the pylons, targeting pod, and the finned store has caused the agreement to deteriorate. The computed results still follow the trend of the measured results, but agreement in detail is not as good as before, particularly with regard to the orifices between the pylons.

In the region beneath the aircraft, the agreement between the computed and measured results is reasonable for the two configurations shown. The pressure agreement for the clean aircraft, Fig. 8, is fair to good and the sidewash, $\arctan(v/u)$, and upwash, $\arctan(w/u)$, comparisons, Figs. 9 and 10, are quite good. With the addition of the pylons, targeting pod, and store (Figs. 11–13), the agreement is still fair, except in the wake region. However, even in the wake region, Figs. 11c and 12c show the comparisons to be acceptable. (The disparity in the comparison made in the wake of the store shown in Fig. 13c is out of character with the other comparisons.) Of particular interest are the sidewash distributions in Figs. 9b and 12b because the flow angle is important when computing store trajectories. Note the steepening of the sidewash angle at the traverse position near the outboard pylons as the pylons and stores are added. (The store occupies the x position from approximately FS 414 to 546.) This steep change in sidewash from fore to aft is indicative of a yawing moment on the store positioned nearby. Change in upwash angle is relatively small, but well predicted in Fig. 13b. Most important, the agreement between the measured and computed distributions is still good for engineering purposes. For instance, measurement of the yawing moment coefficient in the tunnel gave a value of 6.857 in the direction that would move the nose of the store away from the fuselage centerline. The computed value was 6.360.

Further evidence of the engineering quality of the computed results is afforded by predictions of the trajectory of the store, Fig. 14. Both the data curve and the solid curve of Fig. 14 were determined in the same manner. The six-degree-of-freedom equations of motion were integrated numerically using the changing aerodynamic loads on the store at each increment of the trajectory. After release, the aerodynamic forces were deduced from the flowfield by the influence coefficient method.[9] However, the data curve is produced from wind-tunnel information and the solid curve is determined entirely from the Euler flowfield solution. The two trajectories of the respective centers of gravity are indistinguishable. Yaw and roll agree very well, but the pitch-up apparent in the curve from the wind-tunnel data is not as well predicted out away from the aircraft.

Conclusions

The maturation of the domain decomposition method coupled with an accurate inviscid three-dimensional flow solver has allowed the calculation of the flowfields about complex configurations. In the present work, this method was used on a wing/body/inlet configuration with six pylons, a targeting pod, and a finned store in its carriage position on one pylon. The comparisons with wind-tunnel measurements show the calculated flowfields to be of the same character as those obtained in the wind tunnel. In an absolute sense, the quality of the comparisons between calculated and measured results were good for a configuration of wing/body/inlet, but as pylons and stores were added, the quality of the comparisons diminished, as would be expected with an inviscid solver. Still,

the comparisons are of sufficient quality to aid in the making of engineering decisions while in the design process, particularly with regard to store placement. A major benefit of the techniques employed is that once grid generation has been completed, change to elements or the addition of elements is easily accomplished.

Acknowledgments

The work reported herein was conducted by the Arnold Engineering Development Center (AEDC), Air Force Systems Command, at the request of Aeronautical Systems Division, Wright-Patterson Air Force Base, Ohio. The results of the research were obtained by Calspan Corporation/AEDC Operations, operating contractor for the aerospace flight dynamics testing program at AEDC.

References

[1]Benek, J. A., Buning, P. G., and Steger, J. L., "A 3-D Chimera Grid Embedding Technique," AIAA Paper 85-1523, July 1985.

[2]Dietz, W. E., Jacocks, J. L., and Fox, J. H., "Application of Domain Decomposition to the Analysis of Complex Aerodynamic Configurations," *Third International Symposium on Domain Decomposition Methods for Partial Differential Equations*, edited by T. F. Chan, R. Glowinski, J. Periaux, and O. B. Widlund, Society for Industrial and Applied Mathematics, Philadelphia, March 1989, pp. 428–450.

[3]Beam, R., and Warming, R. F., "An Implicit Finite-Difference Algorithm for Hyperbolic Systems in Conservation-Law Form," *Journal of Computational Physics*, Vol. 22, No. 1, Sept. 1976, pp. 87–110.

[4]Pulliam, T. H., and Steger, J. L., "Implicit Finite-Difference Simulations of Three-Dimensional Compressible Flow," *AIAA Journal*, Vol. 18, No. 2, 1980, pp. 156–169.

[5]Thompson, J. F., "Program EAGLE Numerical Grid Generation System User Manual Vol. III: Grid Generation System," Air Force Armament Lab., Eglin AFB, FL, TR-87-15, March 1987.

[6]Akima, H., "A Method of Smooth Curve Fitting," Institute for Telecommunications Sciences, Boulder, CO, Environmental Science Services Administration TR-ERL101-ITS 73, Jan. 1969.

[7]Fox, J. H., Donegan, T. L., Jacocks, J. L., and Nichols, R. H., "Computation of the Euler Flow Field Produced by a Transonic Aircraft with Stores," AIAA Paper 89-2219, Aug. 1989.

[8]Thompson, J. F., et al., "Interactive EAGLE: An Interactive Surface Mesh and Three-Dimensional Grid Generation System," AIAA Paper 90-1569, June 1990.

[9]Keen, K. S., "Inexpensive Calibrations for the Influence Function Method Using the Interference Distributed Loads Code," AIAA Paper 85-0270, Jan. 1985.